Journal of Constructional Steel Research 66 (2010) 19–27

Contents lists available at ScienceDirect

Journal of Constructional Steel Research

journal homepage: www.elsevier.com/locate/jcsr

The effect of stiffeners on the strain patterns of the welded connection zone

Roozbeh Kiamanesh [a], Ali Abolmaali [a,*], Mehdi Ghassemieh [b]

[a] 'UT-Arlington Center for Structural Engineering Research, University of Texas at Arlington, Arlington, TX, 76019, United States

[b] Department of Civil Engineering, University of Tehran, Tehran, Iran

ARTICLE INFO

Article history:
Received 23 April 2009
Accepted 17 July 2009

Keywords:
I-Beam to Box-column
Force transfer mechanism
Steel Connection
Seismic
Cyclic
Energy dissipation
Hysteresis
Stiffener
Hardening

ABSTRACT

The behavior of the welded I-beams to box-columns connections is investigated both experimentally and numerically to identify the effects of stiffeners and column flange thickness on the energy dissipation characteristic of the connection. Numerical test specimens were developed and analyzed by the finite element method and the results were compared with full-scale experiments. The effects of various stiffeners such as, column stiffeners, side-stiffeners, and top-flange, and bottom-flange stiffeners were investigated. The contribution of each stiffener in controlling the location of the plastic deformation and the energy dissipation in the connection zone were examined.

1. Introduction

The use of I-beam to box-column connection (IB–BC) in the steel moment resisting frame structures (Fig. 1) is increasing because of the inherent strength properties, when subjected to multi-directional loading [1]. The parameters affecting the performance of the connection are: type and size of the stiffeners, column size, beam size, the column versus beam stiffness, the slenderness of the beam and column elements, and the welding material residual stresses. Any or combinations of these parameters can significantly alter the behavior and performance of the connection [2].

White and Fang [3] and Chen and Lin [4] studied the effects of both internal and external stiffeners on the behavior of IB–BC connections. They concluded that the connections with triangular stiffeners have the lowest rigidity while those with side-stiffeners present significantly higher moment-rotation capacity. Shanmugam et al. [2] studied 15 different IB–BC connections with various stiffeners and monitored the stress distribution at the web of the box-column and the flange of I-beam. Among the connections tested, the connections with side-stiffeners exhibited higher ductility. Ghobadi et al. [5] investigated the performance of the retrofitted connections with side-stiffeners. The results showed an improvement in the ductility of the connection while eliminating the crack propagation at the connection zone. Design guidelines were proposed based on full-scale experiments and finite element analyses. The results indicated that connections with sufficient stiffeners satisfy the basic seismic design criteria and provide sufficient strength, stiffness, and rotation capacity [6,7].

The benefits of using side-stiffeners were also studied by Shin et al. [8] and Kang et al. [9] on concrete filled tabular (CFT) columns connected to I-beams. Most tests conducted on the CFT connection with side-stiffeners showed stable hysteresis and adequate ductility.

The objective of this study is to build on previous studies and to investigate the stress and strain distribution and load transfer mechanism in the stiffeners of the IB–BC connections under cyclic loading by varying critical connection variables in order to optimize the connection details and control its cyclic performance. Thus, a nonlinear 3D finite element model was used to model and to simulate the performance of the connection. This study particularly focuses on: (1) the connections with and without column stiffeners; (2) variation of column flange thickness; (3) variation of top-flange stiffener; and (4) variation of side-stiffener.

2. Experimental testing

Following the AISC Seismic Provision [10] and the FEMA design capacity procedure [11], Ghobadi et al. [12] performed five full-scale tests on the improved and retrofitted IB–BC connection specimens to investigate the effect of the weld size on the connection. These connections were fabricated in pairs in order to verify the cyclic response of the specimens.

Among the five moment resisting connections tested by Ghobadi et al. [12], only one failed prematurely due to early fracture of

* Corresponding author. Tel.: +1 817 272 3877; fax: +1 817 272 2630.
E-mail address: abolmaali@uta.edu (A. Abolmaali).

0143-974X/$ – see front matter © 2009 Elsevier Ltd. All rights reserved.
doi:10.1016/j.jcsr.2009.07.010

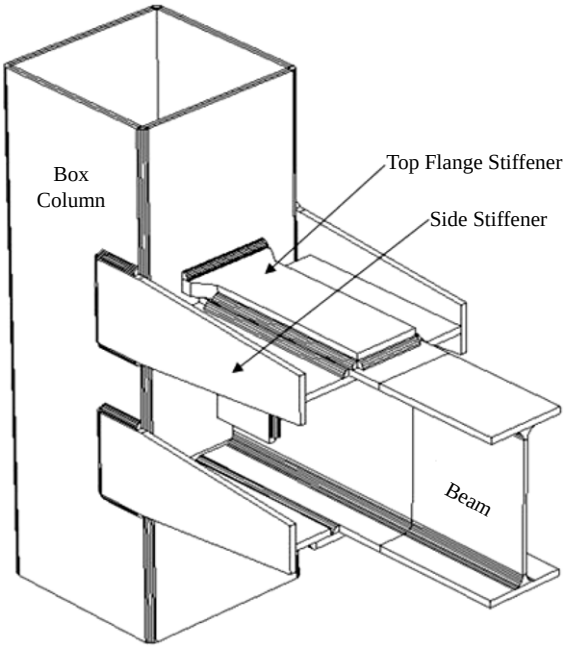

Fig. 1. A Typical I-beam to box-column connection.

the single fillet weld of the top flange. Two of the specimens failed due to lateral torsional buckling and fracture in the beam flange. The other two specimens sustained the cyclic loads for the story drift in excess of more than 5% before the failure occurred.

In this study, the experimental results of RC3 and RC4 introduced by Ghobadi et al. [12], and RC7 by Ghobadi et al. [5] were used for the finite element verification. Fig. 2 illustrates the details of the RC3. which is stiffened and retrofitted with the side-stiffeners. The RC4 connection is fabricated with 8 mm (5/16 in.) double fillet weld. The details of this connection are presented in Fig. 3.

The specimen RC7 was designed and tested by Ghobadi et al. [5] with a factor of 1.2 for the calculation of plastic moment capacity of the beam. The RC7 connection contained column stiffeners, top and bottom beam flange stiffeners, and side-stiffeners. The various stiffeners included in this connection provide the capability of removing the stiffeners or altering the stiffener thickness while maintaining the stability and effectiveness of the connection. Ghobadi et al. [5] also investigated the seismic performance and ductility of RC7 when the connection was retrofitted by a side-stiffener. Fig. 4 shows the details of the Connection RC7. The geometric details of the test specimens RC3, RC4, and RC7 are presented in Table 1.

A typical test setup presented by Ghobadi et al. [5] and Ghobadi et al. [12] is shown in Fig. 5 and a typical experimental specimen is presented in Fig. 6. A concentrated load was applied at the tip of the 2520 mm (99.2 in.) column using a 500 kN (112.5 kips) hydraulic jack with the maximum stroke of ±200 mm (±8 in.). Specimens were subjected to the cyclic displacement history in accordance with the FEMA [11] as shown in Fig. 7. The tip displacement corresponding to a story drift ratio of 0.01 rad was 26 mm (1.02 in.). The results of the coupon tensile test of all the components of the connections are shown in Table 2.

3. Finite element model analysis

The finite element method was used to model the connection assembly and to investigate the stress and strain distribution patterns in the connection stiffeners. The finite element software ABAQUS 6.8-1 [13] with the capability of performing both geo-

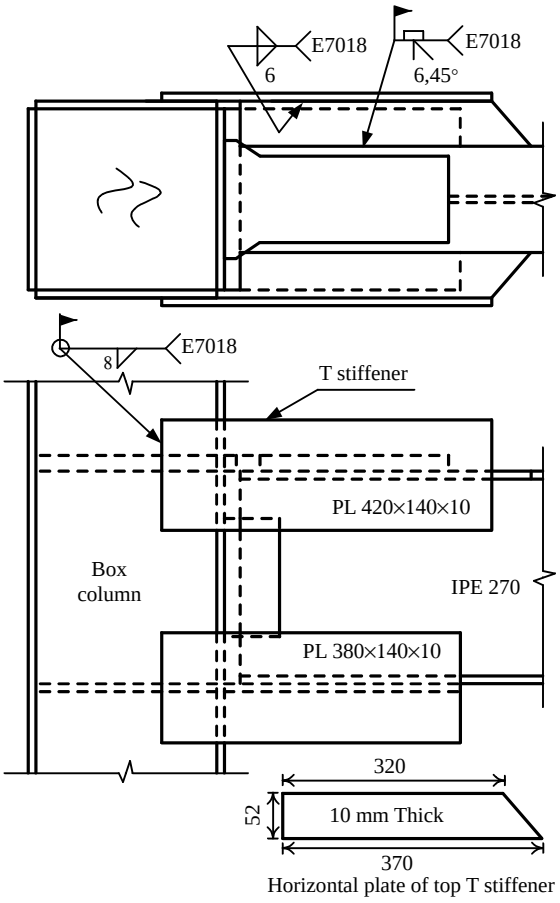

Fig. 2. Connection details of specimen RC3, Ghobadi et al. [12].

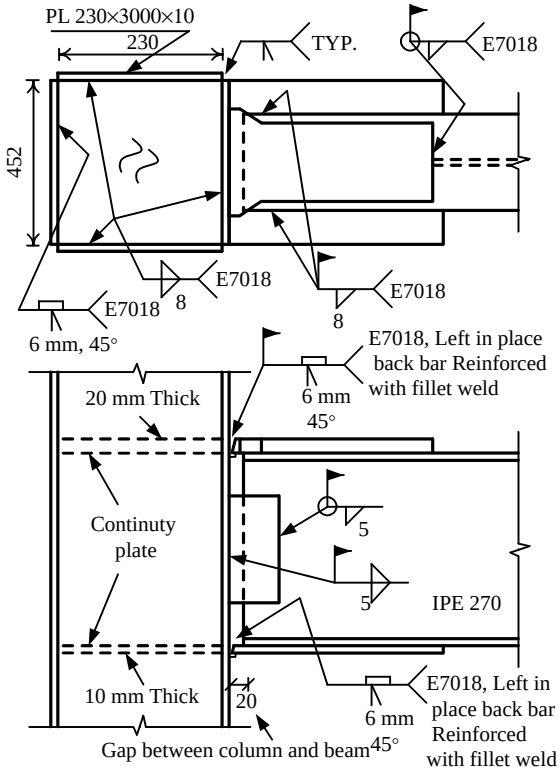

Fig. 3. Connection details of specimen RC4, Ghobadi et al. [12].

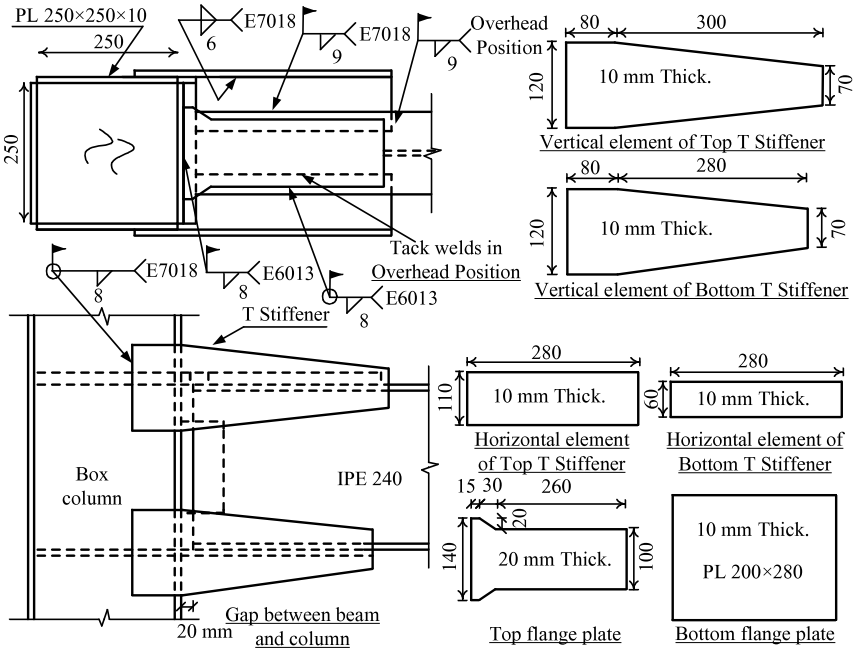

Fig. 4. Connection details of specimen RC7, Ghobadi et al. [5].

Table 1
The details of experimental tests.

Connection	Beam size	b mm (in.)	t_f mm (in.)	h mm (in.)	t_w mm (in.)	Column size mm (in.)	T-Stiffener
RC3	IPE-270	135 (5-5/16)	10 (3/8)	270 (10-5/8)	7 (1/4)	230 (9)	Rectangular
RC4	IPE-270	135 (5-5/16)	10 (3/8)	270 (10-5/8)	7 (1/4)	230 (9)	W/O
RC7	IPE-240	120 (4-3/4)	10 (3/8)	240 (9-7/16)	6 (1.4)	250 (9-13/16)	Tapered

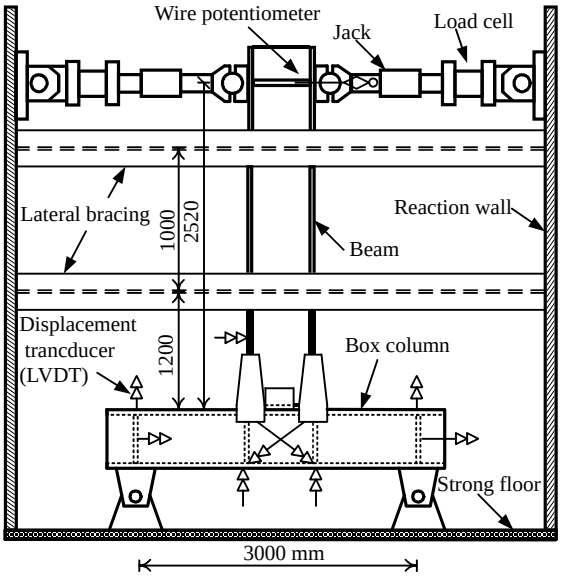

Fig. 5. Full-scale test setup and instrumentation, Ghobadi et al. [5], [12].

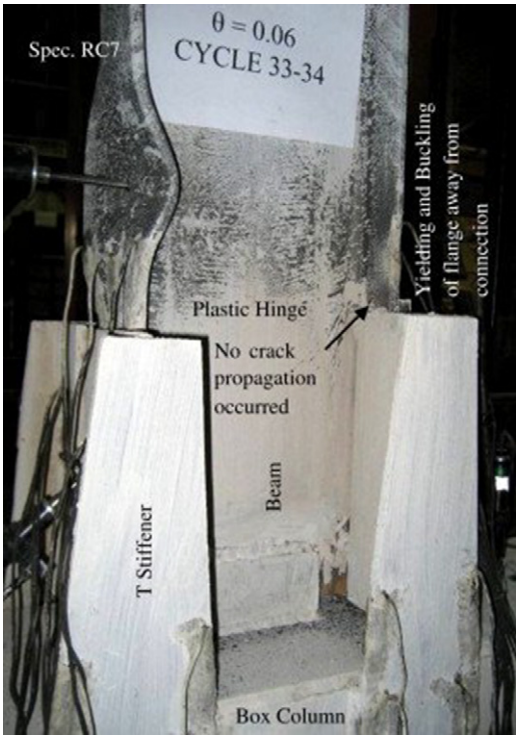

Fig. 6. Typical experimental specimen, Ghobadi et al. [5].

metric and material nonlinear analyses was used to model the connection. The beam, column, and stiffeners were meshed and discretized by 4-noded linear tetrahedral (C3D4) and 8-noded linear brick (C3D8R) elements with reduced integration and hourglass control. The tetrahedral elements were used in the complicated areas such as connection zone where the size of the mesh was reduced to 15 mm (0.59 in.). The brick elements were used elsewhere in the model, and the size of the mesh was gradually increased up to 60 mm (2.36 in.) at the regions with small elastic strains. The details and locations of the elements for a typical finite element model are illustrated in Fig. 8.

Table 2
Tensile coupon test results.

Test coupon	F_y MPa (ksi)	F_u MPa (ksi)	F_y/F_u	Elongation (%)
Beam web (ST37-2)	334 (48.4)	464 (67.3)	0.71	30
Beam flange (ST37-2)	311 (45.1)	438 (63.5)	0.71	26
Column plate, bottom-flange plate and T-stiffener (10 mm Thickness)	320 (46.4)	460 (66.7)	0.69	27
Top-flange plate (20 mm Thick.)	267 (38.7)	424 (61.5)	0.63	27

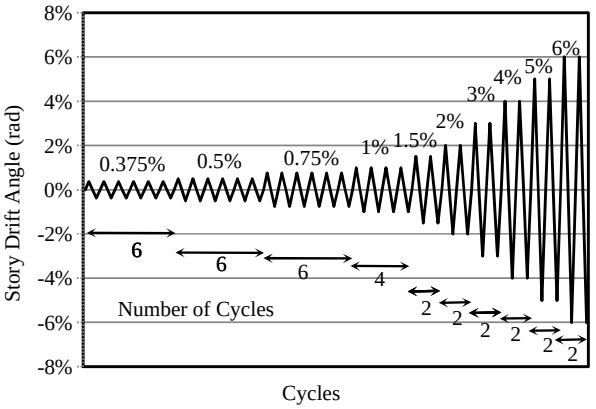

Fig. 7. Cyclic loading history, FEMA 350.

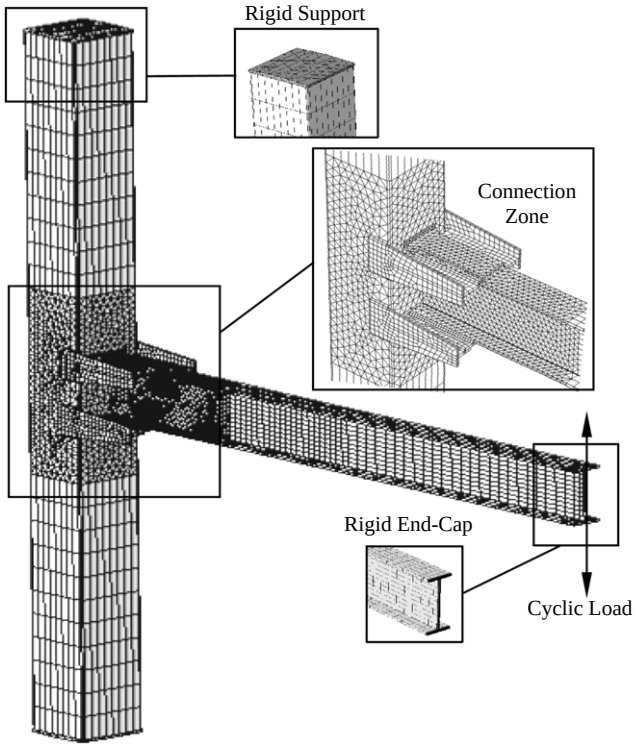

Fig. 8. Typical finite element model, and mesh properties. (18 000 elements, typical computation time: 4 h).

A rigid part (un-deformable mesh regions) was attached to the tip of the beam and both ends of the column to simulate a rigid beam end cap which distribute the load caused by the cyclic displacement control evenly at the tip of the beam (Fig. 8). The column end caps simulate the pin support to simulate the boundary condition of the test setup as illustrated in Fig. 8.

Table 3
Material properties.

Parameter	Value
C MPa (ksi)	14 000 (2030)
γ	140
Q_∞ MPa (ksi)	1800 (261)
B	0.26

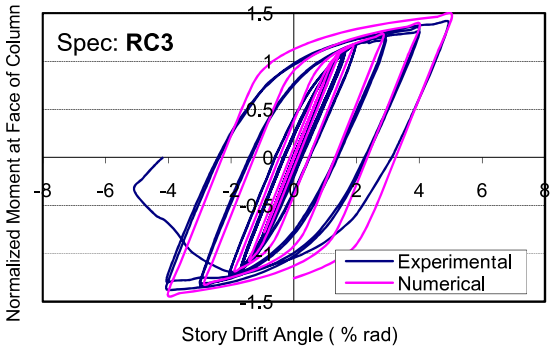

Fig. 9. Cyclic responses of specimens RC3.

The combined hardening plasticity model was used in order to model the material behavior during the cyclic loading. The parameters for combined strain hardening was selected from the material property reported by Ghobadi et al. [12] and the rate of hardening used in the FEM was calibrated after several attempts such that the numerical analysis results replicated most accurately the experimental results.

The algorithm used for the combined hardening of the low-carbon material in ABAQUS 6.8-1 is based on the study conducted by Doghri et al. [14], which is capable of performing both kinematic and isotropic hardening. The kinematic hardening parameters C and γ are defined as the initial hardening modulus and the rate at which the hardening modulus increases with increasing plastic strain, respectively. The isotropic hardening behavior of the material is modeled with exponential law. The parameters Q_∞ and b are defined as the maximum increase in the plastic range and the rate at which the maximum size is reached when plastic strain develops, respectively. The values of the combined strain hardening parameters used in this research are tabulated in Table 3. A Young's modulus of $E = 210$ GPa (30×10^3 ksi) and a Poisson's ratio of $\upsilon = 0.3$ were used to define the elastic response of the material with $\sigma_y = 310$ MPa (44.9 ksi).

The FEM results for the normalized beam moment at the column face to the beam plastic moment (M/M_p) versus story drift angle (θ) for the tests designated by Ghobadi et al. [12] as RC3 and RC4; and Ghobadi et al. [5] as RC7 are presented in Figs. 8 through 10. These figures reveal that the hysteresis loops obtained from the numerical analysis have slightly sharper corners than those of the experimental results while the ultimate load and initial stiffness are accurately simulated. The same behavior was also observed by Shin et al. [15] who suggested that this behavior is due to disregarding the residual stresses during the numerical analysis.

The connection RC3 failed by lateral torsional buckling due to insufficient bracing before the completion of cyclic loading history. Therefore, the finite element analysis was stopped manually at the same loading stage that the specimen failed during the test.

Table 4 compares the energy dissipation obtained from the finite element analysis with those from the experiments. The maximum error in energy dissipation value was 6% when comparing the experimental and FEM results.

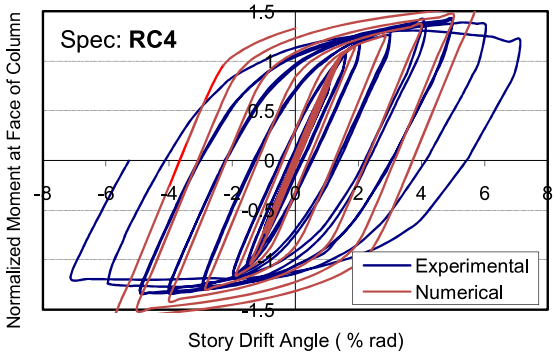

Fig. 10. Cyclic responses of specimens RC4.

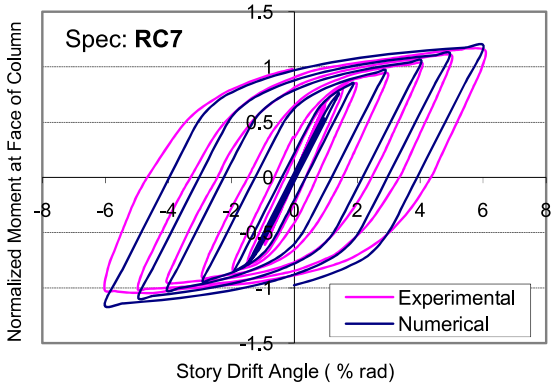

Fig. 11. Cyclic responses of specimens RC7.

Table 4
Energy dissipated of each connection kN.m-rad (kip.ft-rad).

Model	Experimental	Finite element	Error (%)
RC3	101.3 (74.7)	107.4 (79.2)	6
RC4	298.0 (219.8)	297.2 (219.2)	1
RC7	245.5 (181.0)	233.0 (171.8)	4.8

Table 5
Range of element thickness and designated symbols.

Element	Symbol	Range mm (in.)
Column thickness	C	8 (5/16), 10 (3/8), 12 (1/2)
Side-stiffener	SS	5 (3/16), 10 (3/8)
Top-flange stiffener	TFS	20 (3/4),10 (3/8), 0 (0)
Column stiffener	CS	W, WO

4. Finite element results

Parametric studies were conducted to identify the effects of the stiffeners and column thickness on the connection behavior. Ting et al. [1] studied the effect of various stiffeners on the performance of the IB–BC connections and suggested that the connections with column stiffeners have similar moment-rotation characteristics as those without column stiffeners and with side-stiffeners when they are subjected to monotonic loading. The same behavior was also observed in this study in which cyclic load was applied. Thus, the parametric study was conducted only on the connections without column stiffener.

The values of the column stiffeners, top-flange stiffener, and side-stiffeners were varied to monitor the effect of each component on the connection performance. The values of column plate thickness used were 8, 10, and 12 mm (5/16, 3/8, and 1/2 in.), while the thickness value of the top-flange stiffener was 10 mm (3/8 in.) and 20 mm (3/4 in.). The connection behavior with and without top-flange stiffener was also investigated. Two thickness values of 5 mm (3/16 in.) and 10 mm (3/8 in.) were selected for the side-stiffeners. The range and the relative symbols of each parameter are tabulated in Table 5. The hysteresis loops for each connection model was obtained for applied moment versus beam end-rotation and the area under its enveloping curve defining the energy dissipation characteristics of the connection was calculated. The model designation and the values of the energy dissipation of the FEM models for different connections are presented in Table 6.

The model C10-SS10-TFS20-WCS is the finite element model of RC7 with column plate thickness of 10 mm (C10), side-stiffener of 10 mm (SS10), top-flange stiffener of 20 mm (TFS20), and it is with column stiffeners (WCS). The energy dissipation of the RC7 obtained from the experimental results (245.5. kN.m-rad, 181 kip.ft-rad) is in close agreement with the FEM results (233.0 kN.m-rad, 172 kip.ft-rad). A close examination of the results presented in

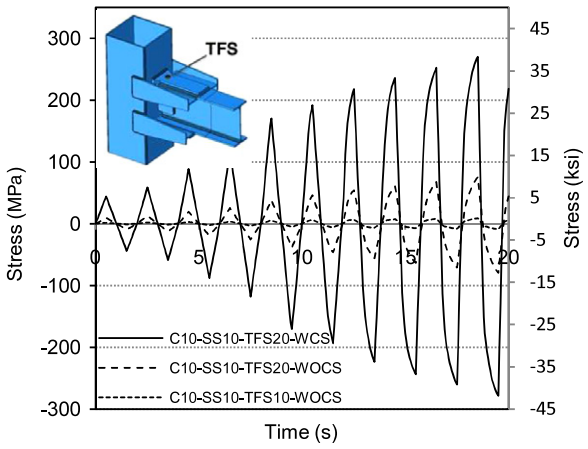

Fig. 12. Stress history at top-flange stiffener.

Table 6 shows more than 19% reduction in energy dissipation of the connection when the column stiffener was removed; compare C10-SS10-TFS20-WCS and C10-SS10-TFS20-WOCS. In C10-SS10-TFS20-WCS, majority of the load transfers from the top-flange stiffener to the column stiffener; however, by removing the column stiffener in C10-SS10-TFS20-WOCS the load is rerouted to the column through the side-stiffeners, which undergoes plastic deformation. This phenomenon is explained in more detail in the next section.

5. Stress history

5.1. Effect of top-flange stiffener and column stiffener

Three stressed regions were selected on the top-flange stiffener, side-stiffener, and the beam flange to study the response of the connection when the values of the stiffeners\thickness were varied. Fig. 12 shows a high stress concentration at the region of top-flange stiffener when column stiffener is included (C10-SS10-TFS20-WCS). However the stresses in the top-stiffener drop significantly when the column stiffener was removed (C10-SS10-TFS20-WOCS). The stress reduction in top-flange stiffener was calculated to be in excess of 95% during the last loading cycle. This indicates that direct stress transfer from the top-flange stiffener to the column occurs when the column stiffeners are included. The further reduction of stresses in the beam's top-flange stiffener is noticed when its thickness is reduced from 20 mm (3/4 in.) to 10 mm (3/8 in.).

The examination of Fig. 13 shows a significant stress increase in the side-stiffener when the column stiffener was removed (compare C10-SS10-TFS20-WCS with C10-SS10-TFS20-WOCS). More than 90% stress increase was calculated during the peak of the

Table 6
Model name and the relative energy dissipation. Name, kN.m-rad (kip.ft-rad).

SS mm (in.)		TFS mm (in.)	C mm (in.)		
			8 (5/16)	10 (3/8)	12 (1/2)
10 (3/8)	WCS	20 (3/4)		C10-T10-TFS20-WCS 233.0 (171.8)	
	WOCS	20 (3/4)	C8-SS10-TFS20-WOCS 181.3 (133.7)	C10-SS10-TFS20-WOCS 188.5 (139.0)	C12-SS10-TFS20-WOCS 197.2 (145.4)
		10 (3/8)	C8-SS10-TFS10-WOCS 178.4 (131.6)	C10-SS10-TFS10-WOCS 184.8 (136.3)	C12-SS10-TFS10-WOCS 195.3 (144.0)
		N/A	C8-SS10-TFS0-WOCS 176.3 (130.0)	C10-SS10-TFS0-WOCS 182.7 (134.7)	C12-SS10-TFS0-WOCS 189.6 (139.8)
5 (3/16)	WCS	20 (3/4)		C10-SS5-TFS20-WCS 227.9 (168.0)	
	WOCS	20 (3/4)	C8-SS5-TFS20-WOCS 187.3 (138.1)	C10-SS5-TFS20-WOCS 199.7 (147.2)	C12-SS5-TFS20-WOCS 200.4 (147.8)
		10 (3/8)	C8-SS5-TFS10-WOCS 181.5 (133.8)	C10-SS5-TFS10-WOCS 188.7 (139.1)	C12-SS5-TFS10-WOCS 195.6 (144.3)
		N/A	C8-SS5-TFS0-WOCS 179.6 (132.5)	C10-SS5-TFS0-WOCS 185.5 (136.8)	C12-SS5-TFS0-WOCS 190.8 (140.7)

C: Column, SS: Side-Stiffener, TFS: Top-Flange Stiffener, WCS: With Column Stiffener, WOCS: Without Column Stiffener.

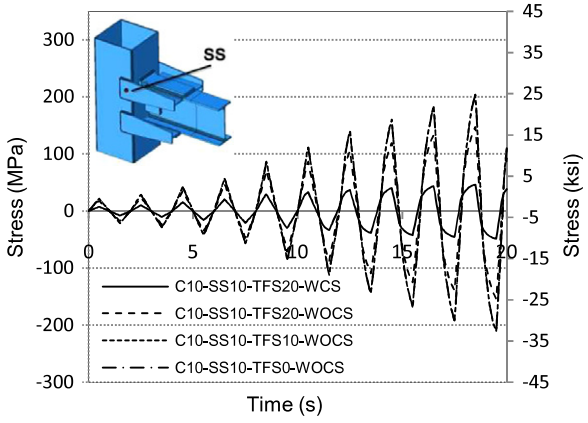

Fig. 13. Stress history at the side-stiffener.

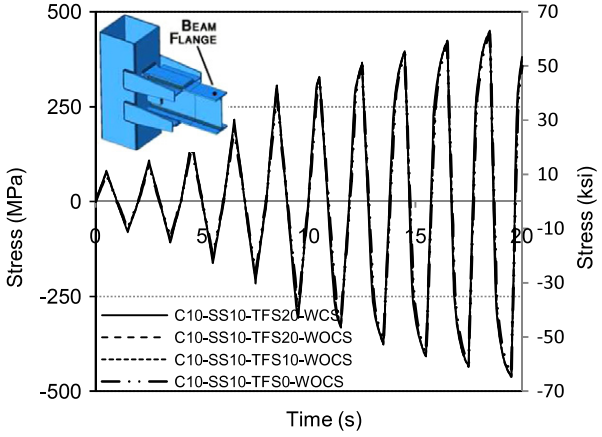

Fig. 14. Stress history at beam's top flange.

last loading cycle when the column stiffeners were removed. Also the stress level in the side-stiffener was gradually increased when the thickness of top-flange stiffener was reduced. By removing the top-stiffener, the stress in the side-stiffener increases by 37% and 40% when comparing the models with 20 mm (3/4 in.) and 10 mm (3/8 in.) top-flange stiffeners, respectively.

Fig. 14 shows the location where stresses are obtained in the beam's top flange. These results show a similar stress history in the beam's top flange regardless of the connection details. Since the beam has less stiffness than the connection and the column, the majority of the energy absorption occurs in the connection by forming the plastic hinge in the beam. This is in accordance with the FEMA-350 [11] that suggests the reduced beam section philosophy which forces the plastic deformation to occur at the beam end. The hysteresis loops of RC7 obtained from the experimental testing presented in Fig. 11 indicated that the moment response of the connection is approaching the plastic moment capacity of the beam. Thus, the moment capacity of the connection is limited by the plastic moment capacity of the beam (M_p) when the column and connection are stiffer than the beam.

5.2. Effect of column thickness

Relative increase in the stresses at the top-flange stiffener was observed when the column thickness was increased within the selected range as shown in Fig. 15. In the absence of column stiffener, the forces transfer from the top-flange stiffener to the box-column,

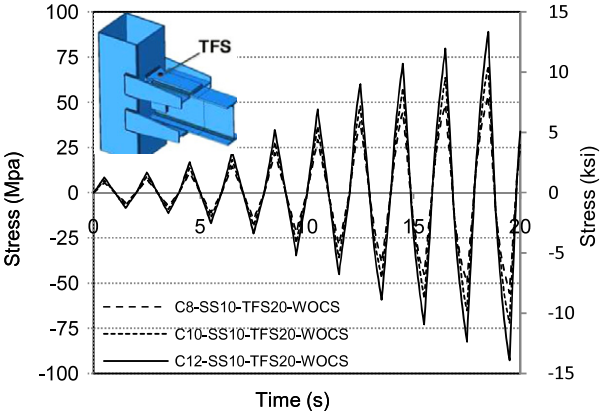

Fig. 15. Stress history at beam's top-flange stiffener.

which causes the column plate deformation in the direction of the force that reduces the stress level in the top-flange stiffener. Theoretically, increasing column thickness increases the stiffness of the column which consequently increases the stress level in the top-flange stiffener. This behavior was also observed in the FEM analysis in which the value of stresses increased by 70% and 140% when the thickness increased from 8 mm (5/16 in.) to 10 mm (3/8 in.) and 8 mm (5/16 in.) to 12 mm (1/2 in.), respectively (see Fig. 15). The stress increase in the beam's top-flange stiffener accordingly results in the decrease of the stress in the side-stiffener. This effect is illustrated in Figs. 15 and 16.

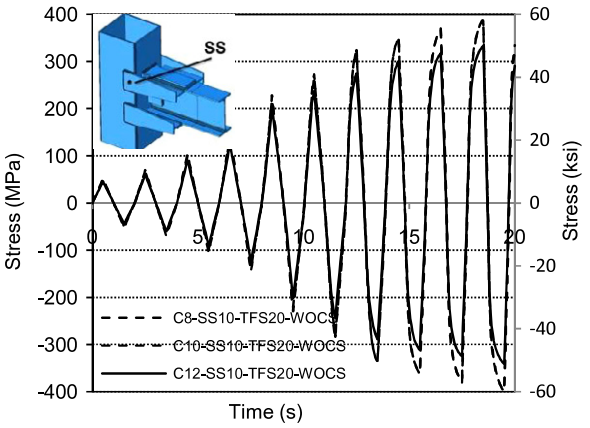

Fig. 16. Stress history at side-stiffener.

The connections with 8 mm (5/16 in.) column thickness and 5 mm (3/16 in.) side-stiffeners were subjected to localized plastic deformation at the column flange and side-stiffener, which assisted the beam end in carrying the plastic strain. This reduced the beam end yielding and consequently its rotation which in turn reduces the energy dissipation.

6. Strain pattern

The equivalent plastic strain (PEEQ) contours of the models during the peak of the last cyclic loading are illustrated in Figs. 17 and 18, which are formatted with the same arrangement as Table 6 for the 5 mm (3/16 in.) and 10 mm (3/8 in.) side-stiffeners, respectively. The vertical groups represent the connections with the same column thickness while the horizontal groups show the models with the same top-flange stiffener configuration. The dark regions indicate that the plastic strain in the element exceeds the yield strain of the materials. Figs. 17(a) and 18(a) are the models with column stiffeners. It can be seen from these figures that removing the column stiffeners increase the strain in the side-stiffener and column flange significantly.

Comparison of the images grouped vertically (Figs. 17 and 18) shows the strain increases in the side-stiffeners when the thickness of the top-flange stiffener is reduced. This effect is more pronounced in the models with 5 mm (3/16 in.) side-stiffeners (Fig. 17) than the models with 10 mm (3/8 in.) side-stiffeners (Fig. 18). The reduction in the size of the top-flange stiffener also increases the strain in the column flanges. This behavior is more noticeable in the models with thin column flange (compare the vertical groups of Figs. 17 and 18 with 8 mm (5/16 in.) column flange).

The models with smaller side-stiffeners (5 mm (3/16 in.)) undergo a large plastic deformation in their side-stiffeners (Fig. 17) which contributes toward inelastic energy dissipation of the connection. Thus, the beam end yielding reduces when comparing Fig. 17 with Fig. 18 (connections with 10 mm (3/8 in.) side-sti-

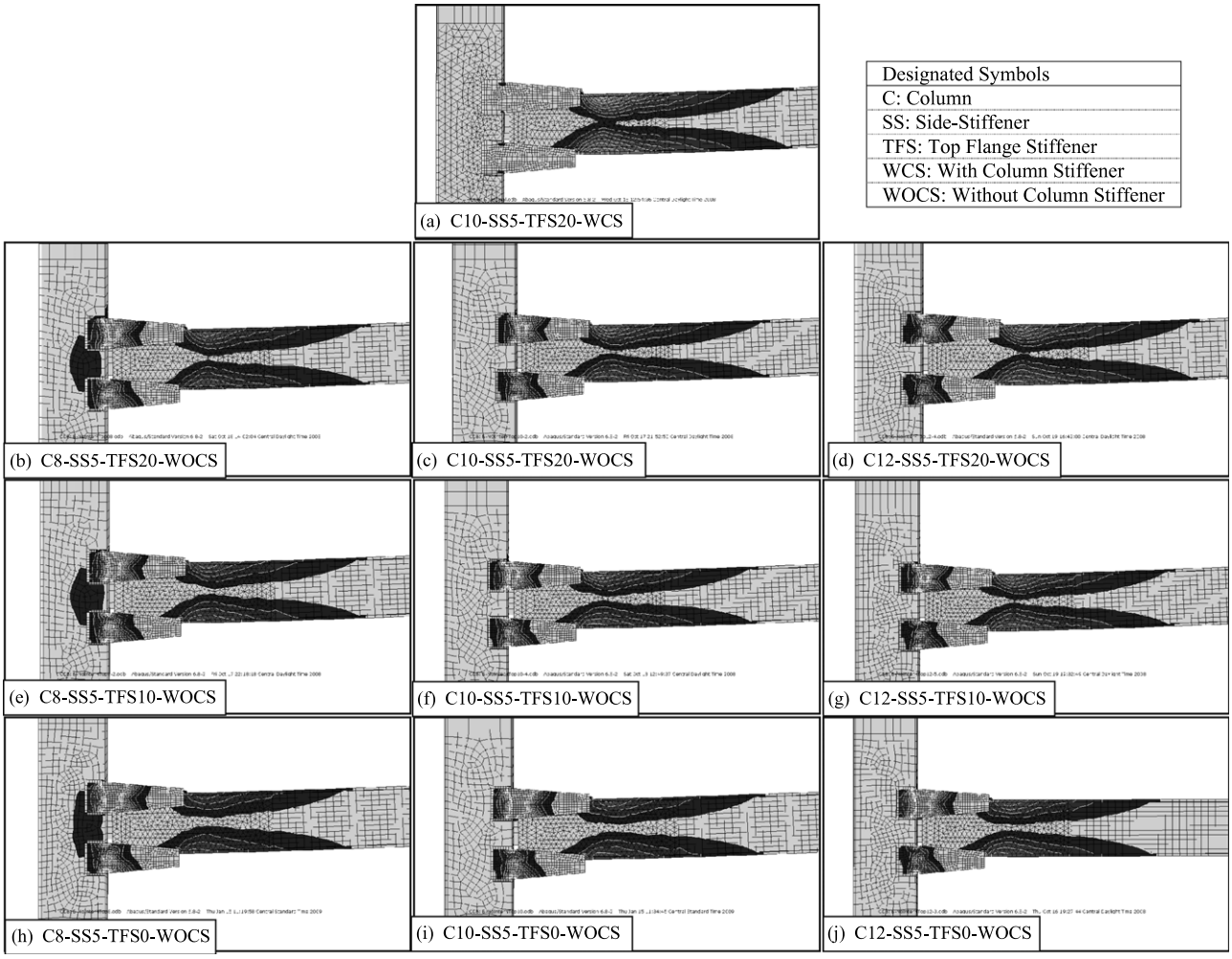

Fig. 17. PEEQ contour when the thicknesses of the T-stiffeners are 5 mm (3/16 in.).

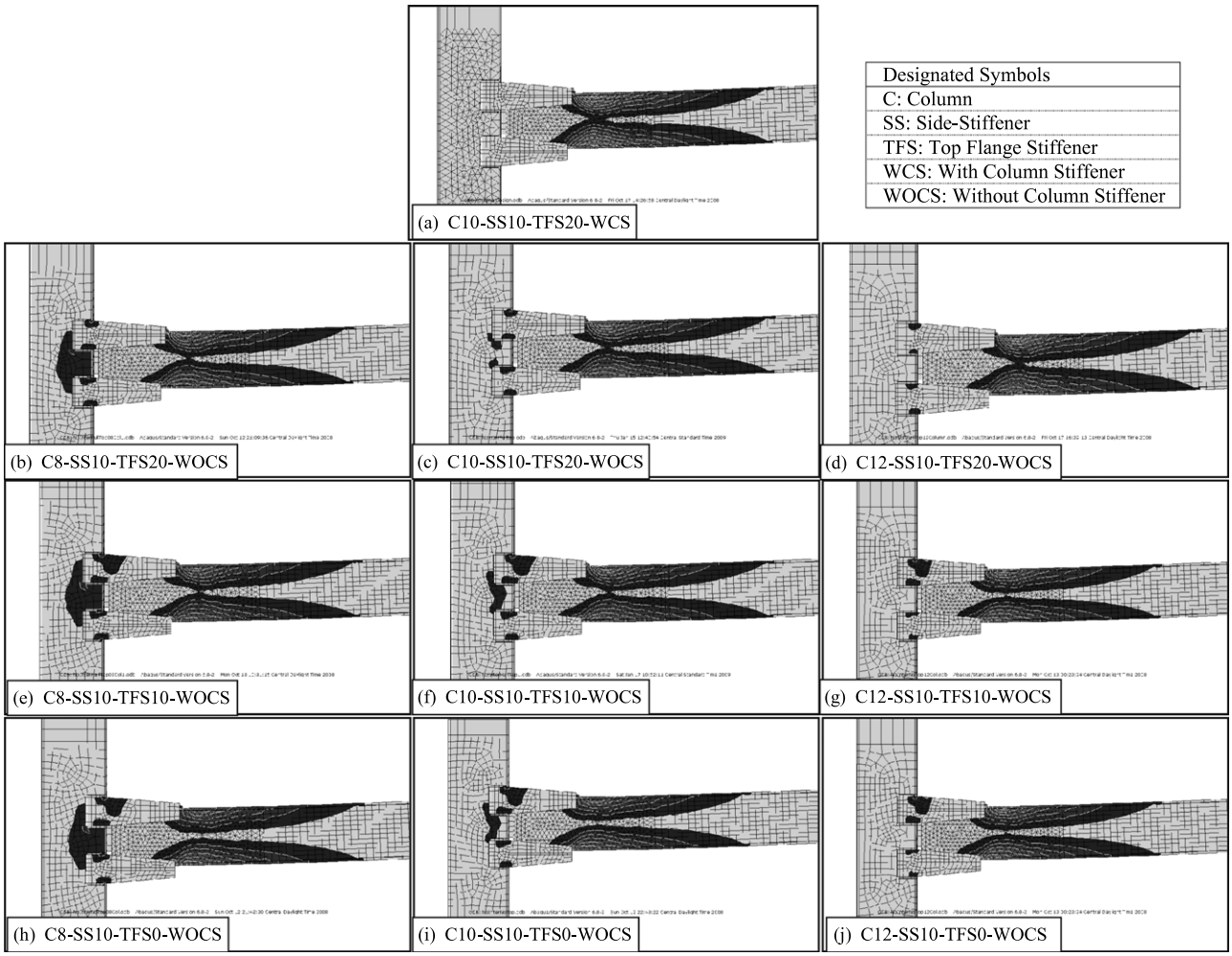

Fig. 18. PEEQ contour when the thicknesses of the T-stiffeners are 10 mm (3/8 in.).

ffeners). It is interesting to note that the level of yielding and plastic deformation of the beam and column can be controlled and adjusted by varying the size of the top- and side-stiffeners. As the size of the top-stiffener reduces, the side-stiffeners activate to assist transferring the stress from the beam to the column, and depending on their size (thickness) they control the yielding of the beam end and column.

For example, the 10 mm (3/8 in.) side-stiffeners with 10 mm (3/8 in.) top-stiffener in C8-SS10-TFS10-WOCS has reduced the beam yielding when compared with C8-SS10-TFS20-WOCS which has 20 mm (1/2 in.) top-flange stiffener. This phenomenon was observed in all cases with different intensity depending on the size of the side-stiffener and the column flange thickness.

It is also noted that the size of the side-stiffener is highly effective in the yielding of the column depending on the size of the column flange. The side-stiffener with higher thickness undergoes less deformation and directly transfers the stress from the beam to the column. This can be observed by comparing Fig. 17(c), (f), and (i) with Fig. 18(c), (f) and (i) for medium column with 10 mm (3/8 in.) thickness.

7. Conclusion

The behavior of an IB–BC connection is investigated both experimentally and numerically. A parametric study was conducted on 20 finite element models to investigate the effect of stiffeners on the connection hysteresis, load transfer mechanism, and stress and strain patterns of the connections.

Forcing the plastic deformation to the beam end is a desirable and a common practice in seismic moment resisting frames. This is achieved by increasing the relative stiffness of the column and connection with respect to beam end. This study introduced the alternative methods to control the location and intensity of the plastic deformation in the connection zone. This will enable designers to properly adjust the connection stiffeners and/or column thickness for informed seismic design.

The models with both column stiffeners and top-flange stiffeners had the highest value of energy dissipation. The results of the stress analysis show that the majority of the load transfers from the top-flange stiffeners to the column when the column stiffener is in place. In these models the side-stiffeners had minimum stress with no evidence of plastic strain. Also the results indicate that the beam top-flange stiffener is significantly effective when it is incorporated with the column stiffeners. A significant stress reduction in the top-flange stiffener was observed when the column stiffener was removed.

The results show that the load path shifts from the top-flange stiffener to the side-stiffener when the column stiffener was removed. A stress increase and large plastic strain are observed in the side-stiffeners when the column stiffener was removed. Therefore when the column stiffener does not exist, the size of the side-stiffener becomes critical, and it should be a major design consideration.

Decreasing the column thickness in general decreases the stiffness of the connection. This phenomenon relocates a portion of the plastic deformation from the beam end to the column and/or side-stiffeners.

References

[1] Ting LT, Shanmugam NE, Lee SL. Non-Linear analysis of I-beam to box-column connection. Journal of Construction Steel Research 1994;28(3):257–78.

[2] Shanmugam NE, Tin LT, Lee SL. Behavior of I-beam to box-column connections stiffened externally and subjected to fluctuating loads. Journal of Construction Steel Research 1991;20(2):129–248.

[3] White RN, Fang PJ. Framing connections for square structural tubing. In: National engineering conference. 1695. p. 74–102.

[4] Chen SJ, Lin HY. Experimental study of steel I-Beam to Box-Column moment connection. In: 4th international conference on steel structures and space frames. 1990. p. 41–7.

[5] Ghobadi MS, Ghassemieh M, Mazroi A, Abolmaali A. Seismic performance of ductile welded connections using T-stiffener. Journal of Constructional Steel Research 2009;65(4):766–75.

[6] Lee SL, Ting LC, Shanmugam NE. Use of external T-stiffeners in box-column to I-beam connections. Journal of Construction Steel Research 1993;26(2–3): 77–98.

[7] Ting LC, Shanmugam NE, Lee SL. Design of I-beam to box-column connections stiffened externally. AISC Engineering Journal 1993;30(4):141–9.

[8] Shin KJ, Kim YJ, Oh YS, Moon TS. Behavior of welded CFT column to H-beam connections with external stiffeners. Engineering Structures 2004;26: 1877–87.

[9] Kang CH, Shin KJ, Oh YS, Moon TS. Hysteresis behavior of CFT column to H-beam connections with external T-stiffener and penetrate elements. Engineering Structures 2001;23:1194–201.

[10] AISC. Seismic provisions for structural steel buildings. Chicago (IL) American Institute of Steel Connection; 2005.

[11] FEMA recommended seismic design criteria new steel moment frame building. Report no. FEMA-350. Federal Emergency Management Agency; 2000.

[12] Ghobadi MS, Mazroi A, Ghassemieh M. Cyclic response characteristics of retrofitted moment resisting connection. Journal of Constructional Steel Research 2008;65(3).

[13] ABAQUS version 6.8-2 user's manual. Michigan: Hibbit, Carlson & Sorensen Inc.; 2008.

[14] Doghri I, Benallal A, Billardon r. An integration algorithm and the corresponding consistent tangent operator for fully coupled elastoplastic and damage equations. Communications in Applied Numerical Methods 1988;(4): 731–40.

[15] Shin KJ, Kim YJ, Oh YS, Moon TS. The behavior of welded CFT column to H-beam connection with external stiffeners. Engineering Structures 2004;26: 1877–87.